Published in final edited form as:
Biochemistry. 2012 July 24; 51(29): 5791–5803. doi:10.1021/bi300391m.

The Catalytic Zinc Site and Mechanism of the Metalloenzyme PR-AMP Cyclohydrolase

Robert L. D'Ordine, **Rebecca S. Linger**[‡], **Carolyn J. Thai**, and **V. Jo Davisson**[*]
Department of Medicinal Chemistry and Molecular Pharmacology Purdue University, West Lafayette, IN 47907-1333

Abstract

The enzyme N^1-(5'-phosphoribosyl) adenosine-5'-monophosphate cyclohydrolase (PR-AMP cyclohydrolase) is a Zn^{2+} metalloprotein encoded by the *hisI* gene. It catalyzes the third step of histidine biosynthesis (Scheme 1), an uncommon ring opening of a purine heterocycle for use in primary metabolism. A three dimensional structure of the enzyme from *Methanobacterium thermoautotrophicum* has revealed that three conserved cysteine residues occur at the dimer interface and likely form the catalytic site. To investigate of the functions of these cysteines in the enzyme from *Methanococcus vannielii,* a series of biochemical studies were pursued to test the basic hypothesis regarding their roles in catalysis. Inactivation of the enzyme activity by methyl methane thiosulfonate (MMTS) or 5,5'-dithiobis(2-nitrobenzoic acid) (DTNB) also compromised the Zn^{2+} binding properties of the protein inducing loss of up to 90% of the metal. Overall reaction stoichiometry and the potassium cyanide (KCN) induced cleavage of the protein suggested that all three cysteines were modified in the process. The enzyme was protected from DTNB-induced inactivation by inclusion of the substrate PR-AMP while Mg^{2+}, a metal required for catalytic activity, enhanced the rate of inactivation. Site directed mutations of the conserved C93, C109, C116 and the double mutant C109/C116 were prepared and analyzed for catalytic activity, Zn^{2+} content, and reactivity with DTNB. Substitution of alanine for each of the conserved cysteines showed no measurable catalytic activity and only the C116A was still capable of binding Zn^{2+}. Reactions of DTNB with the C109A/C116A double mutant showed that C93 is completely modified within 0.5 s. A model consistent with these data involves a DTNB-induced mixed disulfide linkage between C93 and C109 or C116, followed by ejection of the active site Zn^{2+} and provides further evidence that the Zn^{2+} coordination site involves the three conserved cysteine residues. The C93 reactivity is modulated by the presence of the Zn^{2+} and $Mg^{2+}$and substantiates the role of this residue as a metal ligand. In addition, Mg^{2+} ligand binding site(s) indicated by the structural analysis were probed by site-directed mutagenesis of three key aspartate residues flanking the conserved C93 which were shown to have a functional impact on catalysis, cysteine activation, and metal (zinc) binding capacity. The unique amino acid sequence, the dynamic properties of the cysteine ligands involved in Zn^{2+} coordination and the requirement for a second metal (Mg^{2+}) are discussed in the context of their roles in catalysis. The results are consistent with a Zn^{+2} mediated activation of H_2O mechanism involving histidine as a general base that has features similar to but distinct from those of previously characterized purine and pyrimidine deaminases.

[*]Author to whom correspondence should be addressed: V. Jo Davisson, Ph.D., Department of Medicinal Chemistry and Molecular Pharmacology, College of Pharmacy, Purdue University, 575 Stadium Mall Dr., West Lafayette, IN 47907, 765- 494-5238, davisson@purdue.edu.
[‡]Present address: University of Charleston, School of Pharmacy, Charleston, WV

Supplemental materials and additional resources associated with this article are available within the HTML version at http://pubs.acs.org.

Histidine is the only amino acid that derives carbon and nitrogen from another advanced metabolite in the form of ATP. As part of this process, N^1-(5'-phosphoribosyl) adenosine-5'-monophosphate cyclohydrolase (PR-AMP cyclohydrolase) encoded by the *hisI* gene maintains the unique position of promoting the ring opening event of a purine heterocycle for use in primary metabolism, and constitutes the third step of histidine biosynthesis (Scheme 1). This metabolically intense process is dependent upon the utilization of carbon and nitrogen through this hydrolytic event. The potential significance for inhibitor design of this pathway at the level of the PR-AMP cyclohydrolase has been proposed (1–3). Our efforts have focused on a monofunctional enzyme from *Methanococcus vannielii* and established that this enzyme is a metalloprotein containing one high affinity Zn^{2+} per subunit and requiring a free Mg^{2+} ion for catalytic activity (4). There are analogous enzymes belonging to the class of zinc hydrolases that catalyze purine or pyrimidine deamination, for example adenosine(5, 6), cytidine(7), blasticidin S(8), and cytosine deaminases (9). The three-dimensional structures of these enzymes have revealed the details of the zinc coordination (10–17). These enzymes provide specific metal ligands to promote activation of water molecules in the sphere of the zinc atom for attack of the substrate heterocycle(18). However, there are some differences between these deaminases and PR-AMP cyclohydrolase, the foremost being the regiochemistry of the bond cleavage event. PR-AMP cyclohydrolase displays a pH rate profile for k_{cat}/K_m that implicates a single enzyme species with a pK_a of 7.3 (4). This feature is in contrast with those for either cytidine deaminase (pK_a 5.4) (7) or adenosine deaminase (pK_a 4.7) (19). Finally, there is no amino acid sequence homology between the known cyclohydrolases and deaminases implicating distinct evolutionary processes but some elements in common at the level of catalytic mechanism.

Our initial characterization of PR-AMP-cyclohydrolase established that the functional loss of catalytic activity was correlated with an irreversible loss of Zn^{2+} (4). While no evidence for direct involvement of the Zn^{2+} binding site in catalysis was revealed in these previous studies, the functional similarity to the deaminases implicate a role for the metal binding sites in catalysis. Analysis of the sequence conservation in the PR-AMP cyclohydrolases from various organisms provided evidence for potential Zn^{2+} protein ligands. Global alignments of the HisI amino acid sequences by us and others (20) indicate that three cysteine and aspartate residues are invariant in all species and occur in a stretch of highly conserved amino acid residues (see **pfam01502.12)**. The functional importance for the conserved cysteine residues within this region follow from the sequence analysis of the known *E. coli* UTH903 *hisI(-)* mutant (21). DNA sequencing of this mutant indicated that the *hisIE* gene had undergone a point mutation that rendered a C to F change at the third conserved cysteine residue.

Despite the apparent significance of these conserved cysteine residues in PR-AMP cyclohydrolase, no functional analyses of these residues have been reported. The discovery of the metalloprotein character of the enzyme from *M. vannielii,* and the recent three dimensional structure of the *Methanobacterium thermoautotrophicum* protein indicating cysteine residues from separate monomers making the Zn^{2+} binding site, motivated a working hypothesis for evolution of the catalytic site at the dimer interface (22, 23). All three of the conserved cysteines are implicated in coordination of the metal in a Cd^{2+} substituted form of the protein. An additional metal binding site for a Mg^{2+} ion was also proposed based upon the known requirement for catalytic activity and the proximity to the putative Zn^{2+} binding site.

The distinctive features of the active site in the PR-AMP cyclohydrolase implicated role(s) for the conserved cysteines in catalysis. By using chemical modification and analysis of site-directed mutants of the invariant cysteine and histidine residues as well as some other key

aspartate residues in the *M. vannielii* PR-AMP cyclohydrolase, the reactivity and essential features of the amino acids in metal binding were evaluated. The unique amino acid sequence and the dynamic properties of the cysteine Zn^{2+}ligands are discussed in the context of their likely direct role(s) in catalysis. We also establish experimental evidence for the functional roles of three aspartate residues in metal binding and propose a catalytic mechanism consistent with a distinct zinc hydrolase family.

MATERIALS AND METHODS

Materials

All chemicals, buffers, resins and general enzymes were purchased from commercial sources. Custom oligonucleotides were synthesized by the Purdue Campus facility. DNA preparation was performed using commercial kits. Desalting and concentration of proteins were completed using commercial centrifugal filters.

General Methods

All procedures, restriction digests, transformation of *E. coli,* end-labeling, and general molecular biology manipulations were carried out using standard protocols (24, 25). *E. coli* DH5α or XL-1 Blue were used as host strains for propagation of plasmid DNA. Manual DNA sequencing of the mutant constructs was performed using a commercial cycle sequencing kit with end-labeled T7 primer. After separation of DNA sequencing reaction fragments on an 8% PAGE urea gel, the results were imaged on a phosphorimager. Complete DNA sequencing of the mutant *hisI* genes was performed using fluorescent 5'Cy5 end-labeled primers (standard T7 or T3 primers) and cycle sequencing.

Protein concentrations were determined by the method of Bradford (26). SDS-PAGE was run under reducing conditions using Tris-Tricine gels as described previously (4). UV-Vis spectrophotometry , stopped-flow spectrophotometry and MALDI-MS were performed in house. Atomic absorption analyses of protein samples for Zn^{2+} content were conducted at the Indiana State Chemist Laboratory.

Amino Acid Sequence Alignments

All amino acid sequences presented here were taken from the available databases (DNA and protein) at the National Center for Biotechnology Information (NCBI). Homologous sequences were identified using BLAST sequence search algorithm (27, 28). Sequence alignments provided were produced using ClustalW (v1.6) (29) after initial alignment by Pile-Up (30, 31).

Mutant Preparation

The C93A, C109A, C116A, and H110A mutants were produced using the megaprimer PCR (32) method while the C109A/C116A, D92E, D94E, and D94A mutants were produced using the sight overlap extension method (33). The C109A/C116A double mutant was produced in succession utilizing the C116A mutant as template for the C109A change. When possible these changes were chosen to incorporate or remove unique cleavage sites to allow for initial screening by DNA restriction analysis.

The native primers, which contained restriction sites in non-coding regions, were as follows: *M. vannielii hisI* (Sense) 5′-GCA TGA ATT CAT ATG GGC ATT AAA GAC ATT-3′, (Antisense) 5′-GGG CAA GCT TCA TTA ATC TAG TTT ATC TCC-3′. These primers were designed with *Eco*RI and *Nco*I sites and a start codon in the sense primer and a *Hind*III site and a stop codon in the antisense primer. Sense strand mutant primers, where the underlined codon indicates the position of the mutation, were used for C93A 5′-GAA GTA

TTT AAA GAC GCG GAT GGT GAT GCC CTC-3′, C116A 5′-GGA TAT ATG TCA GCT TTT CAT AAT AAA-3′, H110A 5'-GCA TGG GCA TGT GCA GAA GGA TAT ATG-3'; and D94A 5'-GTA TTT AAA GAC TGT GCA GGT GAT GCC CTC-3'. In a similar fashion, antisense primers were used for C109A 5′-ATA TCC TTC ATG AGC TGC CCA TCC AGT-3′. D92E 5'-ATC ACC ATC ACA TTC TTT AAA TAC TTC-3'; and D94E 5'-GAG GGC ATC ACC TTC ACA CTG TTT AAA-3'.

All final products were cloned into pBluescript II SK(+) using the *Eco*RI and *Hind*III restriction sites and selected recombinants were analyzed by DNA restriction and sequence analysis. The site directed mutations were confirmed using a [^{32}P]-end labeled primer and the Cycle Sequencing kit (Promega). The entire coding sequences of the *hisI* mutant clones were then established using the general DNA sequencing methods. The *Nco*I-*Hind*III restriction fragments encoding each mutant *hisI* were ligated into the same sites of pET-28(b)+ to create the desired *hisI* mutant expression constructs.

Overproduction of Protein, Purification, and Assay of PR-AMP Cyclohydrolase

Overproduction, purification and assay of *PR-AMP cyclohydrolase* was carried out using the procedure previously described (4). Since many of the mutants possessed no catalytic activity, SDS-PAGE was used to follow the elution of the mutant proteins at each step of the purification. These samples were concentrated, filtered through a 0.22 μm low protein-binding filter, and stored at 4 °C until use.

PR-AMP Cyclohydrolase Inactivation by Cysteine Modification

Fresh solutions of MMTS (methyl methane thiosulfonate) and recrystallized DTNB (5,5'-dithiobis(2-nitrobenzoic acid)) were used for inactivation studies with PR-AMP cyclohydrolase. MMTS inactivation reactions contained 2.0 μM enzyme in 50 mM Tris-HCl pH 7.5, 0.5 mM EDTA and varied concentrations of MMTS. When substrate, PR-AMP was present in reactions it was at 1.1 mM. The experiments were initiated by the addition of MMTS to the protein sample at 4 °C. Samples (10 μL) were taken at specified time intervals, immediately diluted into 1 mL of assay buffer, and analyzed using the standard enzyme assay conditions. Pseudo first order rates of inactivation were estimated from the percent activity as a function of time. All initial rates were estimated in duplicate and parallel controls were run for all samples.

The inactivation of PR-AMP cyclohydrolase by DTNB was executed in 50 mM Tris-HCl pH 7.5, 1mM EDTA, 10 mM Mg2+ at 20 °C. To a sample of PR-AMP cyclohydrolase (2.0 μM) at 20 °C was added DTNB (106 μM to 296 μM), and when appropriate 1.1 mM PR-AMP was included. At indicated times, 10 μL aliquots of these mixtures were removed and immediately diluted into 1 mL assay buffer and analyzed for catalytic activity. Estimates of the inactivation rates were derived as described above.

To compare the rates of TNB^{2-} (nitro-5-thiobenzoate anion) formation with those for enzyme inactivation, TNB^{2-} formation was monitored in separate experiments using the conditions as described above. DTNB was mixed with PR-AMP cyclohydrolase (9.0 μM) to final concentrations of 585 μM, 981 μM or 1.36 mM and formation of TNB2- was observed at 412 nm for the full course of the reaction. The data were fit to either single or double exponential functions using Origin 5.0 software to arrive at estimates of the rate constants.

Samples of the MMTS and DTNB inactivated PR-AMP cyclohydrolase were submitted for metal analysis (see below). The samples were allowed to react for up to 1 h at which point less than 0.01 % the catalytic activity remained.

Stoichiometry of DTNB Modification

The stoichiometry of modification by DTNB for native and mutant PR-AMP cyclohydrolases was determined by incubation of varied enzyme concentrations (9.7 μM to 23.4 μM) with 30 to 100 fold molar excess DTNB, in 50 mM Tris-HCl pH 8.5, 1mM EDTA, 5–10 mM Mg^{2+} at 30 °C. All PR-AMP cyclohydrolase preparations used in these determinations were buffer exchanged by gel filtration chromatography using Superose 12 or Sephadex-G25 columns before analysis. The reactions required from 15–20 minutes for completion. Fresh solutions of recrystallized DTNB were used for all stoichiometry experiments and a determination of the extinction coefficient for TNB^{2-} under these conditions yielded 13, 830 M^{-1} cm^{-1} (34).

The DTNB modified PR-AMP cyclohydrolase was subjected to gel filtration over Superose 12 or Sephadex-G25 to remove excess DTNB. These samples were then reacted with KCN (5–10 mM) in the same buffer as above to release TNB^{2-}. Release of TNB^{2-} was rapid under these conditions and endpoint absorbances at 412 nm were used to estimate the amount released. Samples of cyanylated-PRAMP cyclohydrolase produced from KCN treatment (or by direct reaction with NTCB) were cleaved at the sites of modification and analyzed by MALDI-MS analysis (35, 36). Briefly, to samples of the cyanylated-PR-AMP cyclohydrolase was added Tris-base (3M), to adjust the pH to 9.0 and the reaction was allowed to react at 37°C for 16h to affect cleavage. Control reactions were untreated protein under the same conditions. The reactions were then diluted 10–50 times with 50% ACN/ 0.1% TFA (1–10 pmol μL-1 protein) and submitted for MALDI-MS to determine the sites of modifications.

Stopped-Flow Kinetics

The initial rate estimates of TNB^{2-} formation for reactions of DTNB with native PR-AMP cyclohydrolase, the C109A/C116A double mutant species, and free cysteine were determined using a Hi-Tech stopped-flow spectrophotometer. These experiments were executed using a single mixing mode with a stop volume of 110 μL at 20 ± 0.1 °C. Final buffer conditions were 50 mM Tris-HCl pH 8.5, 0.5 mM EDTA 1mM $MgCl_2$ or 50 mM KH_2PO_4 pH 7.3, 0.5 mM EDTA and 1mM $MgCl_2$. After mixing, the reactions contained 440 μM DTNB and 8.7 μM of enzyme or cysteine. The reactions were observed at 412 nm and the resultant data (triplicate) were averaged and fit using a sequential first order rate model in KinetAsyst 2.0 (Hi-Tech, Inc.) to arrive at estimates for the rate constants.

Stopped–Flow Observation of the PR-AMP Cyclohydrolase Reaction

The UV profile for the PR-AMP cyclohydrolase enzymatic reaction was monitored from 220 nm to 340 nm at 23°C using a Hi-Tech stopped-flow spectrophotometer in single-mixing mode. Syringes contained solutions of PR-AMP (4μM) with Mg^{2+} (5mM) and PR-AMP cyclohydrolase (4μM) in 50mM Tris-HCl pH 7.5, 1 mM EDTA. Spectra for the enzyme, product, and substrate starting solutions were acquired. Multivariate analysis of the resultant data was performed using Specfit Software Ver. 2.1.(37, 38)

Metal Ion Analysis

All samples of PR-AMP cyclohydrolase were prepared by extensive dialysis at 4 °C for 2 days prior to metal ion analyses by ICP emission spectroscopy and atomic absorption spectroscopy (AAS). The dialysis bags contained up to 10 mg of protein at 1.0 mg mL^{-1} and equilibrated in 400 mL of 30 mM HEPES pH 7.5 containing 4 g L^{-1} Chelex 100 (50–100 mesh, Na^+ form) resin for 6 to 8 h, followed by changes after 12 to 16 h (2 L) and 30 to 34 h (2L). Spectra/Por 4 12,000–14,000 MWCO dialysis membranes was prepared according to standard procedures (39) and rinsed with HEPES buffer prepared by stirring with 4 g L^{-1}

Chelex 100 for 24 h before use. All HEPES solutions were made from the sodium salt and titrated with NaOH to pH 7.5. All containers (plastic and glassware) were triple rinsed, or soaked in HEPES containing Chelex 100 (4 g L^{-1}) and plastic materials were used whenever possible. As a control to correct for any matrix effects a standard curve was constructed with known quantities of Zn^{2+} from a reference solution of zinc nitrate in the buffer described above. ICP-ES samples (1.5–2.0 mL, 0.5–1.0 mg mL^{-1}) were analyzed at the Chemical Analysis Laboratory (University of Georgia) and AAS samples (7 mL, 0.5–1.0 mg mL^{-1}) were analyzed at the Indiana State Chemist's Laboratory (Purdue University).

Model of PRAMP in the HisI active site—The active site cavity in the crystal structure (22) was defined by 4.5 Å radius around plausible binding site. The PRAMP structure was imported and docked in the active site accounting for distance from Zn required to perform chemistry *i.e.* PRAMP C6 was placed in vicinity of Zn^{2+} as expected for chemistry. Phosphates were placed and modeled in the oxyanion holes that are defined by conserved residues. The flexibility of the ribose rings posed a significant challenge to arrangement of these elements in the active site. After initial substrate placement and several manual iterations the active site and substrate were minimized. This was done by the extending the active site radius to 5 Å and both were locally minimized using default settings for local minimization in ICM pro 3.5 (40).

RESULTS

Amino Acid Alignment of PR-AMP Cyclohydrolase (HisI) Sequences

The alignment in Figure 1 shows that PR-AMP cyclohydrolases across species capable of histidine biosynthesis have three highly conserved cysteines, among twelve other residues that are invariant, in over 95% of the sequences included in the PFAM family (**pfam01502.12)**. As was observed previously (20) (41), these cysteines occur within this highly conserved amino acid motif (the cyclohydrolase motif) found in both the mono-functional and multi-functional histidine biosynthetic enzymes. In *M. vannielii* PR-AMP cyclohydrolase, the three identical positions C93, C109, and C116 are also the only cysteine residues in the protein. The importance of C116 was indicated by the finding that in the *E. coli* UTH903 *hisI(-)* mutant the *hisIE* gene contains the C116F mutation that rendered the HisIE protein inactive (21). Together with sequence conservation, these data implicated key functional roles for the three invariant residues at C93, C109, and C116 in the cyclohydrolase motif and provided further impetus for a focused study.

In addition to the three cysteines, three aspartates and a histidine are also conserved and identical within the PR-AMP cyclohydrolase sequences. Using a composite profile derived from this alignment, [LIV]-x(5)-D-C-D-x-D-x-L-x(7)-[GN]-x(2,3)-C-H-x(4)-[ST]-C-F, the Prosite database (42) was searched for additional homologous sequences, especially those related to known catalytic or metal binding sites, however no homologous sequences were found. More focused comparisons were based upon the possible mechanistic relationships with cysteine proteases and to the reaction catalyzed by adenosine deaminase. Alignments with different forms of adenosine deaminase and AMP deaminase showed no significant similarities with respect to active site residues. The PR-AMP cyclohydrolase sequence contains all residues required for a cysteine protease; a number of papain-like cysteine proteases were aligned using a partial active site signature sequence (43, 44). Sequence alignments based upon the metalloproteases active site pentapeptide motif H-E-X-X-H (45) were also investigated. The results from these efforts failed to reveal any significant relationships between PR-AMP cyclohydrolase and functionally related metalloproteins or cysteine proteases or with any of the described most common active site zinc ligand arrangements (18, 46–49).

Recently, the x-ray crystal structure of the Cd^{2+}-substituted enzyme from *Methanobacterium thermoautotrophicum* was solved and revealed that these residues occur at the dimer interface(22). All of the cysteines and aspartates implicated from the sequence alignments also appear coordinated with Cd^{2+}; one metal coordinates with three cysteines and a second metal with the three aspartates. However, the lack of detectable sequence homology with other zinc hydrolases indicated the cyclohydrolase motif as unique and further motivated detailed biochemical analyses concentrating on the role of the conserved cysteines and the second metal binding site.

Inactivation of PR-AMP Cyclohydrolase by Cysteine Specific Reagents

Our initial focus on the conserved cysteines was to determine how they play a role in the activity of PR-AMP cyclohydrolase. To this end, the inactivation of PR-AMP cyclohydrolase was assayed at varying concentrations of MMTS with and without substrate, PR-AMP. As shown in Figure 2, this reagent in the absence or presence of exogenous Mg^{2+} caused a time dependent inactivation of PR-AMP cyclohydrolase. However, inclusion of the substrate PR-AMP at 1.1 mM protected the enzyme from inactivation 14-fold over enzyme alone at identical concentrations of MMTS. In contrast, 5'-ProFAR (the product) at similar concentrations had only a modest 2-fold impact on the rate of the MMTS inactivation reactions (data not shown).

The thiol modification reagent DTNB was also used to analyze the reactive cysteines in PR-AMP cyclohydrolase (Figure 3). The presence of the substrate PR-AMP also afforded protection to the enzyme reducing the rate 5-fold at identical concentrations of DTNB (Figure 3A). Our previous studies established that Mg^{2+} was required for catalytic activity. In contrast to the MMTS reaction, the rate of the DTNB inactivation was also dependent upon Mg^{2+} shown as a 16-fold enhancement in Figure 3B.

DTNB Reaction Stoichiometry and Sites of Modification with PR-AMP Cyclohydrolase

PR-AMP cyclohydrolase was reacted with DTNB to ascertain the stoichiometry of accessible cysteine residues (Table 1). Samples of the cyclohydrolase with high specific activity (18 U mg^{-1}) resulted in a stoichiometry of 2.0±0.2 moles of TNB^{2-} per mole of subunit. The DTNB modified PR-AMP cyclohydrolase was passed through a gel filtration column and was treated with KCN to release the TNB^{2-} from the modified cysteine residues. However, the mole ratio of TNB^{2-} released was never greater than one cysteine per subunit. To analyze the positions of the DTNB modification, several independent samples were further processed to affect cleavage at the site of cyanylation (35). MALDI-MS analysis of these fragment mixtures provided evidence that all three conserved cysteines in PR-AMP cyclohydrolase could undergo cyanylation; the relative abundance of each site was not determined. The results indicate that DTNB modification can occur at all the sites but with differing frequency. However, incorporation of a third equivalent of DTNB was not observed.

Catalytic Activity, Metal Content, and DTNB Reactions of PR-AMP Cyclohydrolase Cysteine Mutants

Subsequently, we focused on understanding the role of the three conserved cysteines in metal binding and catalysis in PR-AMP cyclohydrolase. The original observations regarding the pH dependence of the steady rate constants implicated a functional group with a pK_a of 7.3 that was required for catalytic activity (4). This functional pK_a was not affected by substitution of the enzyme with Cd^{2+} (22). The chemical identity of this functional group could be a metal-associated water molecule and/or protein metal ligands. In order to directly assess the essential features of the three invariant cysteines, DNA coding sequences in the *M. vannielii hisI* were created that changed these residues to alanine (C93A, C109A,

C116A). In addition, based upon the initial results a double alanine mutant C109A/C116A was also created for this analysis. Each of these mutant proteins were expressed in *E. coli* and purified. In all cases, these proteins showed identical behavior during the purification steps but showed no detectable activity. The location of protein containing fractions was verified by the use of SDS-PAGE electrophoresis. The purified mutants were each tested at levels up to 1000-fold higher than those used for the native enzyme in the standard initial velocity assays. Using the calculated lower limit of detection for this assay, it could be deduced that the cysteine mutant proteins had catalytic activities that were reduced by > 10^4-fold when compared to the native enzyme.

The Zn^{2+} contents of the DTNB modified as well as mutant forms of PR-AMP cyclohydrolase were analyzed using ICP-ES or AAS. Since the cysteine modifying reagents DTNB and MMTS were shown to modify all three conserved cysteine residues, the Zn^{2+} content of the modified wild type PR-AMP cyclohydrolase was analyzed. The results in Table 2 indicate that the cysteine-modified protein had a measurable loss of Zn^{2+} content. To assess the individual roles of the cysteine residues in the metal binding site, the three point mutants and a double mutant were prepared for analysis using identical conditions as those for the native PR-AMP cyclohydrolase samples (Table 2). Mutation of C93 reduced the Zn^{2+} binding affinity so that only trace levels of the metal were detected upon purification of the protein from *E. coli*. In contrast, the single point mutants C109A and C116A showed either a minor reduction or no change in the protein's Zn^{2+} binding capacity. The combined effect of a double mutant C109A/C116A, however, reduced the protein Zn^{2+} binding affinity so that only trace levels of Zn^{2+} were purified with the protein.

Each of the four PR-AMP cyclohydrolase cysteine mutants were tested for their reactivity toward DTNB in a fashion similar to that used for the wild type enzyme. The TNB^{2-} release stoichiometry for these reactions with each of the four mutant proteins is summarized in Table 3. No reaction could be detected with the C93A mutant and DTNB under these conditions. In contrast, the C109A, C116A, and C109A/C116A mutants reacted with DTNB to different extents all less than wild type enzyme. These data are most consistent with the C93 being the most reactive cysteine in the wild type enzyme.

Subsequent reactions with DTNB are likely a mixed pathway involving both intra and inter molecular disulfide exchange with C109 and C116. These results are supported by those data presented in Table 1 for DTNB modification followed by cyanylation of PR-AMP cyclohydrolase. The extent of these disulfide exchange reactions is dependent upon the presence of the other two conserved cysteines, but not Zn^{2+}, since the C109A/C116A mutant was devoid of metal.

Kinetics of DTNB Reactions with Native PR-AMP Cyclohydrolase and Cysteine Mutants

Figure 4A shows the full time course for reaction of native PR-AMP cyclohydrolase with DTNB. The moles of TNB^{2-} anion never exceeded 2 moles per subunit (± 12%) in any preparation, even under denaturing conditions. Curve fitting analysis of these progress curves required at least two kinetic phases with an apparent burst phase that accounted for approximately 0.5 moles per subunit modification within 5 sec (Figures 4A and 4B). The rates for the DTNB reaction with native PR-AMP cyclohydrolase at pH 7.3 could be fit to a consecutive reaction model where the first phase corresponded to approximately 1 mole of TNB^{2-} formation per subunit and occurred within 30 sec at an apparent first order rate of 246 min^{-1}. The second slower phase of DTNB modification was estimated to be 1000-fold slower (0.24 min^{-1}) and accounted for the second mole of TNB^{2-} formation per subunit.

The C109A/C116A mutant which contains a single cysteine (C93) was used in comparative kinetic studies to analyze the reactivity of this cysteine versus that of the native

cyclohydrolase. The kinetics of these reactions with DTNB was compared at two pH conditions. Apparent first order rate constants for the burst phase of these reactions (1.5 s or less) are summarized in Table 4. Figure 4B also shows the stopped-flow traces for the native PR-AMP cyclohydrolase and the mutant enzyme. The apparent first order rate constant of the burst phase with native PR-AMP cyclohydrolase was not significantly different than either C109A/C116A or free cysteine at pH 7.3. However, at pH 8.5, the C109A/C116A demonstrates reaction rate with DTNB that is nearly 10 fold faster than that of free cysteine and 4 fold greater than native PR-AMP cyclohydrolase. In this case, the only residue reacting with DTNB is C93 and there is only trace Zn^{2+} associated with the enzyme (Table 2); the overall stoichiometry of the reaction is 0.87 and is complete within 5s (Table 3 and Figure 4B). Finally, a C93A mutant did not show any reactivity with DTNB (Table 3) supporting the conclusion that C93 is responsible for the initial fast phase accounting for 0.5 moles of the rapid TNB^{2-} formation upon mixing with the native PR-AMP cyclohydrolase.

Under conditions identical to inactivation, the rate of formation of TNB^{2-} with native PR-AMP cyclohydrolase was followed at 412 nm to compare estimates of the first order rate constants for inactivation with the appearance of TNB^{2-}. The second order rate constants for the TNB^{2-} formation and inactivation and were estimated at 0.058 μM^{-1} min^{-1} 0.071 μM^{-1} min^{-1} respectively, indicating that the overall inactivation and TNB^{2-} formation processes were similar.

Analysis of The Mg^{2+} Binding Site

Conserved residues within the 89–117 protein segments are hypothesized to function as a co-catalytic site. The aspartic acid residues in this sequence are seen to coordinate a cadmium ion in the *M. thermoautotrophicum* hisI crystal structure, suggesting they may bind Mg^{2+}, an essential metal for the efficient turnover of the substrate (Figure 1). The protein was also found to undergo an intrinsic change in tryptophan fluorescence upon binding of the product 5'ProFAR; the extent of the fluorescence enhancement was increased 2-fold by inclusion of Mg^{2+} (Supplemental Materials Figure 4). From the structure of the protein, it is clear that one of the two tryptophans is in the active site and is proposed to be involved in substrate stabilization (22). The roles of these aspartic acid residues, which flank C93 were investigated using site-directed mutagenesis and complementation of the $hisI^{-}$ mutant strain of *E. coli* UTH903. The mutant D94A was not able to maintain viability of the strain, while the mutant D94E was able to perform the necessary hydrolysis step with a 2000–fold reduction in k_{cat}/K_m. A second conservative mutation D92E was also analyzed to show a reduction in k_{cat}/K_m by 175-fold from wild type (Table 2). All aspartate mutants resulted in diminished Zn^{2+} binding of 1.4–1.6 fold per subunit (Table 2). These data support a role for D92 and D94 in properly orienting C93 for Zn^{2+} metal coordination (and by structural implication D96).

CD spectra of native and mutant forms of PR-AMP cyclohydrolase were analyzed to determine if the point mutations and alterations in Zn^{2+} content resulted in significant global conformational changes (50). Supplmental Figure 2 shows spectra of five different PR-AMP cyclohydrolase forms. The spectrum of the native form of the enzyme showed features consistent with both α-helix and β-sheet secondary structural content and this was confirmed by recent structure. As expected, a minimum at 205 nm indicating that the secondary structure contains random coil and anti-parallel β-sheet components (51). Overall, the CD spectra of the three single point mutants were nearly identical to the native PR-AMP cyclohydrolase. These data are consistent with a preservation of the global secondary structure in the mutant enzymes.

Analysis of Stopped Flow Kinetic Data for Possible Intermediate

Previous analysis of the full UV-vis spectrum of this reaction progress has shown the presence of three isosbestic points at 223, 247, and 274 respectively. Single turnover reactions were analyzed using stopped-flow analysis of the reaction monitoring from 220 to 310 nm with special attention to the rate of change at the isosbestic points. These data indicated that there are increases and decreases in absorbance consistent with the presence of a detectable intermediate on the path from substrate to product (Supplemental Figure 3). Global fitting of these data indicated the best fits for a two-step model A>B>C with three species including one intermediate (Figure 5 and Supplemental Figure 3). The rates were determined as 23 s^{-1} and 1.4 s^{-1}, respectively and are consistent with the steady-state k_{cat} of 4 s^{-1} at 30 °C.

DISCUSSION

Cysteine Reactivity in PR-AMP Cyclohydrolase

The structure of PR-AMP cyclohydrolase from *M. thermoautotrophicum* (22) indicates that the three cysteines, C93, C109 and C116 (C86, C102 and C109 in *M. thermoautotrophicum*), are interacting with a metal ion at the putative active site of the enzyme. The results presented on the chemical modification of native PR-AMP cyclohydrolase establish that these cysteines are accessible to modification by DTNB (and MMTS) and that substrate protects these cysteines from attack. Free Mg^{2+} does not protect PR-AMP cyclohydrolase; in fact it facilitates reaction with DTNB by either directly activating the enzyme or making cysteine more accessible to attack. Evidence from fluorescence binding studies performed with the enzyme indicated a significant conformational change does take place upon binding substrate in the presence of Mg^{2+}. While MMTS did not show differential reactivity in the presence or absence of exogenous Mg^{2+}, the size differences and relative reactivities of the two reagents are known and their distinctions at the level active site conformation are not unexpected.

Since the cysteine mutants were all catalytically inactive, the reactivity of these cysteines toward DTNB and the metal content were used to assess their roles in metal binding and catalysis. A significant diminution for the reaction of these mutants with DTNB was observed and the presence of C93 was required for reactivity; no attempt was made to further analyze the stoichiometry of the mutant samples by KCN release. However, in the case of the cysteine mutants it was clear that the removal of any cysteine residue resulted in a non-proportional loss of reactivity toward DTNB. This observation is also consistent with the MALDI-MS results for cyanylated enzyme. It is likely that the DTNB label is scrambled after initial attack by the more reactive cysteine and one possible model for these observations can be found in Scheme 2. The amount of TNB^{2-} produced in the reaction with native PR-AMP cyclohydrolase never exceeded 2 moles per subunit (±12%) in any preparation, even under denaturing conditions, indicating either interaction between the cysteines as indicated by Scheme 2 or steric occlusion of the remaining cysteines from reaction. The data further support interpretation of the structural proximity for the cysteines and their functional interdependence at the dimer interface. The reactivity of C93 may be explained by the reduction of its pK_a caused by the flanking aspartate residues (52, 53).

Zinc Binding and Structure Analysis

Cysteines 93, 109, and 116 are all directly involved in metal binding in the PR-AMP cyclohydrolase active site. The three-dimensional structure of Cd^{2+}-substituted HisI substantiated these findings and implicated that Zn^{2+} ion binding at the subunit interface, with C93 coming from one subunit, while C109 and C116 are from the second subunit. The C93A mutant is completely inactive, no reaction with DTNB was observed and Zn^{2+} was

absent from the protein. The C109A/C116A double mutant was also completely inactive, and also lacked the capacity to bind high affinity Zn^{2+}. The single mutants C109A and C116A react partially with DTNB and bind Zn^{2+} to an increasing extent. The presence of Zn^{2+} in the C109A and C116A single mutants influences the reactivity of the second cysteine raising the possibility that the metal increases the relative acidity of these cysteine residues and enhances their reactivity toward disulfide exchange.

Native PR-AMP cyclohydrolase binds a single Zn^{2+} through the three conserved cysteines to function as indicated by the biochemical analysis presented here and is consistent with the Cd^{2+}-substituted crystal structure (22). However, the enzyme is inactive even in the case of C116A where the enzyme has nearly a full complement of zinc demonstrating the importance of all cysteines to the catalytic activity of PR-AMP cyclohydrolase. It is possible that while C116 is in contact with Zn^{2+}, it is not required for metal binding, unlike C109 and C93, which appear to be at least partially necessary to bind a full complement of zinc. In addition, an invariant H110 resides near to these cysteines may also stabilize the site in the absence of one of the other cysteines (except C93). Mutation of H110 to alanine rendered the protein catalytically impaired by a 10^3 reduction in k_{cat}/K_m, however, this species does bind a full complement of Zn^{2+}.

The crystal structure of *M. thermoautotrophicum* hisI places it in the β−grasp fold family of proteins (54) and indicates the dimer interface is formed by two beta strands from one monomer (β1 and β3) packing with β4 from the second monomer. At least 1540 $Å^2$ or ~40% of each monomer's surface area is buried in the dimer interface (22). The two active sites are located at the dimer interface and appear to have potential for some degree of cooperativity which is reflected in the differential kinetics of the DTNB reaction.

Stabilization of Mg^{2+} Binding

In the structure of PR-AMP cyclohydrolase from *M. thermoautotrophicum*, D92 and D94 together with D96 are ligated to a cadmium ion. The location of this metal could correspond to the magnesium binding site. Complementation and kinetic studies of the mutants of these aspartic acids indicate they have a role in catalysis. Indeed, the k_{cat}/K_m values for conservative mutations were decreased 170-fold for D92E, and 2,300-fold for D94E. We propose that these aspartates coordinate magnesium, creating a bend in the loop containing C93, which extends this cysteine into the active site. In addition, the Mg^{2+} ion may play a role in substrate binding at the ribosyl ring of PR-AMP. The loss of complementation seen in the alanine mutants of D92 and D94 (and D96; data not shown) indicates an amplified effect *in vivo* due to the complexity of the environment; suitable levels of magnesium coordination are not achieved in the cellular context reducing substrate binding and catalysis below the threshold for viable histidine biosynthesis.

Substrate Binding Modeling Studies

Based upon the existing protein structure and the additional function data implicating features of the catalytic site, the potential substrate-protein interactions were modeled by docking PR-AMP into the active site. The active site residues were defined by a 4.5 Å radius around the plausible binding site to include 18 key residues of which 16 are invariant and one is functionally conserved among all PR-AMP cyclohydrolases. PR-AMP was imported and docked accounting for the distance required for zinc-activated catalysis. The phosphates were placed and modeled in the oxyanion holes that are defined by conserved residues S67, T68 and S69 for the 5' phosphate and E78, E79 and S80 for the 5 phosphate. After several manual iterations, the active site and substrate were minimized and several key interactions were observed in the resultant structures (Figure 6a) labeled using *Methanococcus vannielii* numbering *(see* Figure 1 alignment). Edge to face pi stacking between W74 and the adenine

ring may assist in substrate binding. The N9 ribosyl group interacts with Mg^{2+} and K22 (R15 in *M. thermoautotrophicum*) resulting in stabilization of the bound substrate. H110 is in a position to pi-stack with the incoming substrate, and potentially has a role in catalysis as a non-essential general base. In the volume between the zinc and the purine ring, a water molecule can be positioned (Figure 6b). The proximity of the zinc-activated water to the site of catalysis on the substrate suggests a major role for C93 in the cyclohydrolase reaction. C6 of the substrate in this docked structure would reside within 2.6 Å of a zinc-activated water.

Active Site Architecture Compared to Cytosine Deaminase

The Zn^{2+} metalloenzyme cytosine deaminase from *S. cerevisiae* has an active site architecture of functional catalytic groups that has similarities to PR-AMP cyclohydrolase, although the backbone connectivity is distinct. In cytosine deaminase, the Zn^{2+} ligands are cysteine and glutamic acid, while two residues, H62 and W152, interact with the bound inhibitor (14). Histidine 110 and W74 are invariant residues that reside within highly conserved regions of the protein. The incoming substrate is proposed to be stabilized by interaction with W74 and oriented for catalysis toward the catalytic zinc (Figure 6a). Ligand-metal interactions in both proteins are within 2.5 Å, indicating that while the cysteines in each protein do not superimpose, they are nevertheless in the proper orientation for zinc coordination.

Proposed Mechanism

From the body of experimental and structural data we propose the following mechanism for the activity of PR-AMP cyclohydrolase. The entering substrate is oriented for catalysis by interaction with two residues, W74 and C93. Cysteine 93 interacts with N6 of the purine ring to hold the substrate in the proper orientation for attack by the zinc-activated water. The substrate is bound in the active site through interaction of the N9-phosphoribosyl with the active site magnesium and edge-face pi-stacking by W74 with the phosphoribosyl ring at N1. The ring opening in PR-AMP cyclohydrolase can be deduced from the structural and dynamic studies of cytosine deaminase (14, 55). Scheme 3 highlights the features of this reaction that are consistent with the current data. The stopped-flow kinetic data revealed the existence of a chemical intermediate on the enzyme with a similar UV extinction coefficient. We interpret these data to be evidence of a tetrahedral intermediate resulting from water addition to the N1-C6 bond of the purine ring system (Scheme 3). The exact stereochemistry of the tetrahedral intermediate cannot be ascertained since inversion is possible at N1 and the lack of constraint on the phosphoribosyl binding interaction not being heavily anchored in the active site (pi-stacking with W74). The attacking water molecule is proposed to be part of the resting enzyme, stabilized by H110 and is activated by the catalytic zinc to attack the purine ring at C6 (Figure 6b). Such a role for histidine has been posited in the structural and mechanistic studies of GTP cyclohydrolase I (56), where mutants lacking this histidine were still able to catalyze the cyclohydrolase reaction, similar to our observations. This functional relationship could explain the apparent pK_a 7.3 in the k_{cat}/K_m values as previously described since protonation of the His110 would render it unable to serve as a general base (4). In kinetic studies of PR-AMP cyclohydrolase from *M. thermoautotrophicum* we obtained a similar pK_a (7.5) to that of the *M. vannielii* protein whether the active site was populated with zinc or cadmium (22) Protonation of the substrate by the zinc-activated water was suggested as a secondary mechanism in the histidine-deficient mutants. Further distinctions from the cytosine and adenosine deaminase reactions is the fact that ammonia is not produced rather a labile C6-N2 bond is cleaved; protonation of the incipient basic N2 group upon formation of the tetrahedral intermediate renders it a good leaving group. The topological relationship in the enzyme active site that allows for the distinction of N2 and N1 positions is still an open question. The active site of the enzyme is

accessible to solvent even when substrate is present and therefore the potential for exchange to facilitate proton transfer is anticipated.

Evolutionary comparisons with the deaminases also indicate some further distinctions from PR-AMP cyclohydrolase. Structural studies of cytosine deaminase from yeast and bacteria indicate this protein underwent convergent evolution, using two separate folds to arrive at the same mechanistic function (15, 16). Whereas the bacterial isoform utilizes the classical $(\beta/\alpha)_8$ barrel, yeast cytosine deaminase has adopted a mixed α/β fold (14, 15). Each monomer of the PR-AMP cyclohydrolase dimer is composed of two antiparallel beta sheets with a single alpha helix placing it in the $\beta-$grasp fold family(54). The structure of PR-AMP cyclohydrolase and the type of metal binding site indicates a functional relationship to other zinc dependent nucleotide deaminases but with clearly distinct features.(57) One significant difference in the PR-AMP cyclohydrolase is the use of three cysteine ligands for coordination of the Zn^{2+} metal which also occurs in select other related enzymes (7, 8, 18, 57, 58). Given the distinctions in the metal binding site ligands, the active site dependence on the dimeric structure, and the additional potential role(s) for Mg^{2+} metal binding sites, a logical proposal emerges that the PR-AMP cyclohydrolase represents a third protein fold that has evolved to function as an amino hydrolase activating water by utilizing zinc.

Supplementary Material

Refer to Web version on PubMed Central for supplementary material.

Acknowledgments

This research was supported by a grant from the National Institutes of Health GM067195 (VJD) and F32GM18083 (RLD)

Abbreviations

AAS	atomic absorption spectroscopy
CD	Circular Dichroism Spectropolarimetry
ddH_2O	double-distilled deionized water
DTNB 5	5'-dithiobis(2-nitrobenzoic acid)
DTT	dithiothreitol
EDTA	(Ethylenedinitrilo) tetraacetic acid
ICP-ES	inductively coupled plasma-emission spectroscopy
HEPES	(N-[2-Hydroxyethyl]piperazine-N'-[2-ethanesulfonic acid])
MALDI-MS	Matrix-Assisted Laser Desorption/Ionization Mass Spectrometry
MMTS	methyl methane thiosulfonate
NTCB	2-nitro-5-thiocyano benzoic acid
PCR	polymerase chain reaction
PR-AMP	N^1-(5'-phosphoribosyl)adenosine 5'-monophosphate
5'-ProFAR	N^1-[(5'-phosphoribulosyl) formimino]-5-aminocarboxamide ribonucleotide adenosine monophosphate
SDS-PAGE	sodium dodecyl sulfate polyacrylamide gel electrophoresis

TAE	Tris Acetate EDTA
TFA	trifluoroacetic acid
TNB^{2-}	nitro-5-thiobenzoate anion
Tris	Tris(hydroxymethly)aminomethane

References

1. Henriksen ST, Liu J, Estiu G, Oltvai ZN, Wiest O. Identification of novel bacterial histidine biosynthesis inhibitors using docking, ensemble rescoring, and whole-cell assays. Bioorganic and Medicinal Chemistry. 2010; 18:5148–5156. [PubMed: 20573514]
2. Lee D-S, Burd H, Liu J, Almaas E, Wiest O, Barabási A-L, Oltvai ZN, Kapatral V. Comparative Genome-Scale Metabolic Reconstruction and Flux Balance Analysis of Multiple Staphylococcus aureus Genomes Identify Novel Antimicrobial Drug Targets. Journal of Bacteriology. 2009; 191:4015–4024. [PubMed: 19376871]
3. Shen Y, Liu J, Estiu G, Isin B, Ahn YY, Lee DS, Barabási AL, Kapatral V, Wiest O, Oltvai ZN. Blueprint for antimicrobial hit discovery targeting metabolic networks. Proceedings of the National Academy of Sciences. 2010; 107:1082–1087.
4. D'Ordine RL, Klem TJ, Davisson VJ. N1-(5'-phosphoribosyl)adenosine -5'-Monophosphate Cyclohydrolase: Purification and Characterization of A Unique Metalloenzyme. Biochemistry. 1999; 38:1537–1546. [PubMed: 9931020]
5. Jones W, Kurz LC, Wolfenden R. Transition-State Stabilization by Adenosine Deaminase:16-Addition of Water to Purine Ribonucleoside The Enzyme's Affinity for 6-Hydroxy-16-dihydropurine Ribonucleoside and the Effective Concentration of Substrate Water at the Active Site. Biochemistry. 1989; 28:1242–1247. [PubMed: 2713361]
6. Merkler DJ, Schramm VL. Catalytic mechanism of yeast adenosine 5'-monophosphate deaminase. Zinc content, substrate specificity, pH studies, and solvent isotope effects. Biochemistry. 1993; 32:5792–5799. [PubMed: 8504099]
7. Carlow DC, Carter CW Jr, Mejlhede N, Neuhard J, Wolfenden R. Cytidine Deaminases from B. subtilis and E. coli: Compensating Effects of Changing Zinc Coordination and Quaternary structure. Biochemistry. 1999; 38:12258–12265. [PubMed: 10493793]
8. Kumasaka T, Yamamoto M, Furuichi M, Nakasako M, Teh AH, Kimura M, Yamaguchi I, Ueki T. Crystal structures of blasticidin S deaminase (BSD): implications for dynamic properties of catalytic zinc. J Biol Chem. 2007; 282:37103–37111. [PubMed: 17959604]
9. Carter CW Jr. The nucleoside deaminases for cytidine and adenosine: structure, transition state stabilization, mechanism, and evolution. Biochimie. 1995; 77:92–98. [PubMed: 7599282]
10. Xiang S, Short SA, Wolfenden R, Carter CW Jr. Transition State Selectivity for a Single Hydroxyl Group During Catalysis by Cytidine Deaminase. Biochemistry. 1995; 34:4516–4523. [PubMed: 7718553]
11. Kuratani M, Ishii R, Bessho Y, Fukunaga R, Sengoku T, Shirouzu M, Sekine S, Yokoyama S. Crystal structure of tRNA adenosine deaminase (TadA) from Aquifex aeolicus. J Biol Chem. 2005; 280:16002–16008. [PubMed: 15677468]
12. Lee W-H, Kim YK, Nam KH, Priyadarshi A, Lee EH, Kim EE, Jeon YH, Cheong C, Hwang KY. Crystal structure of the tRNA-specific adenosine deaminase fromStreptococcus pyogenes. Proteins: Structure, Function, and Bioinformatics. 2007; 68:1016–1019.
13. Luo M, Schramm VL. Transition state structure of E. coli tRNA-specific adenosine deaminase. J Am Chem Soc. 2008; 130:2649–2655. [PubMed: 18251477]
14. Ireton GC, Black ME, Stoddard BL. The 1.14 A crystal structure of yeast cytosine deaminase: evolution of nucleotide salvage enzymes and implications for genetic chemotherapy. Structure. 2003; 11:961–972. [PubMed: 12906827]
15. Ireton GC, McDermitt G, Black ME, Stoddard BL. The structure of *E. coli* cytosine deaminase at 1.5 angstrom resolution. Journal of Molecular Biology. 2002; 513:687–697. [PubMed: 11812140]

16. Ko T-P, Lin J-J, Hu C-Y, Hsu Y-H, Wang AH-J, Liaw S-H. Crystal structure of yeast cytosine deaminase. Journal of Biological Chemistry. 2003; 278:19111–19117. [PubMed: 12637534]
17. Betts L, Xiang S, Short SA, Wolfenden R, Carter CW Jr. Cytidine deaminase. The 2.3 A crystal structure of an enzyme: transition-state analog complex. J Mol Biol. 1994; 235:635–656. [PubMed: 8289286]
18. Reizer J, Buskirk S, Bairoch A, Reizer A, Saier MH Jr. A novel zinc-binding motif found in two ubiquitous deaminase families. Protein Sci. 1994; 3:853–856. [PubMed: 8061614]
19. Van der Weyden MB, Kelley WN. Human adenosine deaminase: distribution and properties. Journal of Biological Chemistry. 1976; 251:5448–5456. [PubMed: 9388]
20. Beckler GS, Reeve JN. Conservation of primary structure in the *hisI* gene of the archaebacterium *Methanococcus vannielii*, the eubacterium *Escherichia coli,* and the eucaryote *Saccharomyces cerevisiae*. Mol Gen Genet. 1986; 204:133–140. [PubMed: 3018439]
21. Garrrick-Silversmith L, Hartman PE. Histidine requiring mutants of *Escherichia coli* K-12. Genetics. 1970; 66:231–244. [PubMed: 4934198]
22. Sivaraman J, Myers RS, Boju L, Sulea T, Cygler M, Davisson VJ, Schrag JD. Crystal structure of *Methanobacterium thermoautotrophicum* phosphoribosyl-AMP cyclohydrolase HisI. Biochemistry. 2005; 44:10071–10080. [PubMed: 16042384]
23. Auld DS. The ins and outs of biological zinc sites. Biometals. 2009; 22:141–148. [PubMed: 19140015]
24. Ausubel, FM.; Brent, R.; Kingston, RE.; Moore, DDASJ.; Struhl, K. Current Protocols in Molecular Biology. Greene Publishing and Wiley Interscience; NY: 1994.
25. Sambrook, J.; Fritsch, EF.; Maniatis, T. Molecular Cloning:A Laboratory Manual. Cold Spring Harbor Laboratory; Cold Spring Harbor NY: 1989.
26. Bradford M. A Rapid and sensitive method for the quantitation of microgram quantities of protein using the principle of dye binding. Anal Biochem. 1976; 72:248–254. [PubMed: 942051]
27. Altschul SF, Gish W, Miller W, Myers EW, Lipman DJ. Basic Local Alignment Search Tool. J Mol Biol. 1990; 215:404–410.
28. Altschul SF, Madden TL, Schaffer AA, Zhang JZ, Miller W, Lipman DJ. Gapped BLAST and PSI-BLAST - A New Generation of Protein Database Search Programs. Nucleic Acids Res. 1997; 25:3389–3402. [PubMed: 9254694]
29. Thompson JD, Higgins DG, Gibson T. CLUSTAL W: Improving The Sensitivity Of Progressive Multiple Sequence Alignment Through Sequence Weighting Position-Specific Gap Penalties And Weight Matrix Choice. Nucleic Acids Research. 1994; 22:4673–4680. [PubMed: 7984417]
30. GCG, P. Wisconsin Sequence Analysis Package Program Manual Version 8. 1994.
31. Feng DF, Doolittle RF. Progressive sequence alignment as a perequisite to correct phylogenetic trees. Journal of Molecular Evolution. 1987; 25:351–360. [PubMed: 3118049]
32. Landt O, Grunert HP, Hahn U. A general method for rapid site-directed mutagenesis using the polymerase chain reaction. Gene. 1990; 96:125–128. [PubMed: 2265750]
33. Ho SN, Hunt HD, Horton RM, Pullen JK, Pease LR. Site-directed Mutagenisis by overlap extension using the polymerase chain reaction. Gene. 1989; 77:51–59. [PubMed: 2744487]
34. Riddles PW, Blakely RL, Zerner B. Reassessment of Ellman's Reagent. Methods enzymol. 1983; 91:49–60. [PubMed: 6855597]
35. Stark GR. Cleavage at Cysteine After Cyanylation. Methods in enzymology. 1977; 47:129–132. [PubMed: 927170]
36. Wu J, Gage DA, Watson JT. A Strategy to Locate Cysteine Residues in Proteins by Specific Chemical Cleavage Followed by Matrix-Assisted Laser Desorption / Ionization Time of Flight Mass Spectrometry. Anal Biochem. 1996; 235:161–174. [PubMed: 8833324]
37. Binstead, RA.; Zuberbuhler, AD. SPECFIT, a global analysis system with expanded factor analysis and Marquardt least squares minimization. 2.1. Spectrum Software Associates; Chapel Hill, NC: 1996.
38. Bracher A, Schramek N, Bacher A. Biosynthesis of pteridines. Stopped-flow kinetic analysis of GTP cyclohydrolase I. Biochemistry. 2001; 40:7896–7902. [PubMed: 11425318]

39. Auld DS. Metal free dialysis tubing. Methods in Enzymology. 1988a; 158:13–14. [PubMed: 3374368]
40. Abagyan R, Totrov M, Kuznetsov D. Icm - a New Method for Protein Modeling and Design - Applications to Docking and Structure Prediction from the Distorted Native Conformation. J Comput Chem. 1994; 15:488–506.
41. Fujimori K, Ohta D. Isolation and characterization of a histidine biosynthetic gene in arabidopsis encoding a polypeptide with two separate domains for phosphoribosyl-ATP pyrophosphohydrolase and phosphoribosyl-AMP cyclohydrolase. Plant Physiology. 1998; 118:275–283. [PubMed: 9733547]
42. Appel RD, Bairoch A, Hochstrasser DF. A new generation of information retrieval tools for biologists: the example of the ExPASy WWW server Prosite server. Trends Biochem Sci. 1994; 19:258–260. [PubMed: 8073505]
43. Storer, ACaMR. Catalytic Mechanism in Papain Family of Cysteine Peptidases. Methods enzymol. 1994; 244:486–500. [PubMed: 7845227]
44. Rawlings, NDaBAJ. Families of Cysteine Peptidases. Methods enzymol. 1994; 244:461–486. [PubMed: 7845226]
45. Rawlings ND, Barrett AJ. Evolutionary families of metallopeptidases. Methods in Enzymology. 1995; 248:183–228. [PubMed: 7674922]
46. Vallee BL, Auld DS. Active site zinc ligands and activated H_2O of zinc enzymes. Proceedings of the National Academy of Science USA. 1990; 87:220–224.
47. Vallee BL, Auld DS. Cocatalytic zinc motifs in enzyme catalysis. Proceedings of the National Academy of Sciences USA. 1993; 90:2715–2718.
48. Vallee BL, Auld DS. New Perspective on Zinc Biochemistry: Cocatalytic sites in Multi-Zinc Enzymes. Biochemistry. 1993a; 32:6493–6500. [PubMed: 8329379]
49. Vallee BL, Auld DS. Zinc: biological function and coordination motifs. Acc Chem Res. 1993b; 26:543–551.
50. Vallee, BL.; Galdes, A. The metallobiochemistry of zinc enzymes. In: Meister, A., editor. Advances in enzymology and related areas of molecular biology. John Wiley & Sons; New York: 1984.
51. van Holde, KE.; Johnson, WC.; Ho, PS. Principles of Physical Biochemistry. Prentice Hall; Upper Saddle River, New Jersey: 1998.
52. Snyder G, Cennerazzo MJ, Karalis AJ, Field D. Electrostatic influence of local cysteine environments on disulfide exchange kinetics. Biochemistry. 1981; 20:6509–6519. [PubMed: 6796114]
53. Britto PJ, Knipling L, Wolff J. The local electrostatic environment determines cysteine reactivity of tubulin. Journal of Biological Chemistry. 2002; 277:29018–29027. [PubMed: 12023292]
54. Burroughs AM, Balaji S, Iyer LM, Aravind L. Small but versatile: the extraordinary functional and structural diversity of the β-grasp fold. Biology Direct. 2007; 2:18. [PubMed: 17605815]
55. Yao L, Sklenak S, Yan H, Cukier RI. A molecular dynamics exploration of the catalytic mechanism of yeast cytosine deaminase. Journal of Physical Chemistry B. 2005; 109:7500–7510.
56. Auerbach G, Herrmann A, Bracher A, Bader G, Gutlich M, Fischer M, Newkamm M, Garrido-Franco M, Richardson J, Nar H, Huber R, Bacher A. Zinc plays a key role in human and bacterial GTP cyclohydrolase I. Proceedings of the National Academy of Science USA. 2000; 97:13567–13572.
57. Goodman RA, Macbeth MR, Beal PA. ADAR Proteins: structure and catalytic mechanism. Current Topics in Microbiology and Immunology. 2012; 353:1–33. [PubMed: 21769729]
58. Ren J, Kotaka M, Lockyer M, Lamb HK, Hawkins AR, Stammers DK. GTP Cyclohydrolase II Structure and Mechanism. J Biol Chem. 2005; 280:36912–36919. [PubMed: 16115872]

A

```
                    S60(67)                    C86(93)           H103(110)
                    *  :   * **  *    .:  .  *** * :       .   **     *:
M.vannielii         STSRNKIWMKGEESKNVQKVLEVFKDCDGDALLFIVEQTGW-ACHEGYMSCFHNKV
M.thermo.           STSRGKLWLKGESSGHVQRVKDVLVDCDGDAVVLKVEQEGG-ACHTGYRSCFYRSI
E.coli              SRTKQRLWTKGETSGNFLNVVSIAPDCDNDTLLVLANPIGP-TCHKGTSSCFGDTA
H.influenzae        SRTKQRLWTKGEISGNFLNVEEMSLDCDNDTLLILVDPIGA-TCHTGEYSCFHQFT
A.thaliana          SRSRSTLWTKGETSNNFINILDVYVDCDRDSIIYLGTPDGP-TCHTGEETCYYTSV
M.jannaschii        STSRKKLWRKGEESGNVQKLIKFYRDCDGDALLFIVEQKGV-ACHEGYYSCFHYKI
M.tuberculosis      SRSRAEQWVKGATSGHTQHVHSVRLDCDGDAVLLTVDQVGG-ACHTGDHSCFDAAV
N.crassa            SR-KRGLWYKGATSGDTQELVRISLDCDNDALKFVVKQKGR-FCHLDQSGCFGQLK
P.pastoris          SR-RHGLWYKGATSGATQKLLGIELDCDGDCLKFVVEQTGVGFCHLERTSCFGQSK
S.cerevisiae        SRSRNEIWIKGETSGNGQKLLQISTDCDSDALKFIVEQENVGFCHLETMSCFGEFK
S.typhimurium       SRTKQRLWTKGETSGLVLNVVSIAPDCDNDTLLVLAKPVGP-TCHKGTSSCFGDAS
```

Numbering based on *M. thermoautotrophicum* crystal structure numbering, *M.vannielii residue numbers in (#).* Lables *=invariant residue;:=highly conserved function. Accession numbers for species in table: *M. vannielii,* X04021; *A. thaliana,* 3461884; *S. cerevisiae,* V01310; *N. crassa,* M27531; *P. pastoris,* X56180; *H. influenzae,* P44503; *S. typhimurium, E. coli,* X03974; *M. tuberculosis,* AD000019; *M. jannaschii,* 2129194,

thermoautotrophicum; 2621294.

B

```
                  **.: *.:   ::::.. *:.::*:**:* *:
M.vannielii MGIKDIDIKENFGKIVQNMDLKFRKIDDKELLIAIAIDKY 40
M.thermo    ----- MIKSK-GDVNILLNFRHN-INGEDLIIAVAQDHE 32
      ruler 1.......10........20........30........40
```

```
                . :***.*:*::*:*: **:**  **:****.*:*:***.

M.vannielii K-NVLMTAFMDKESLKMTLKTGLMHYFSTSRNKIWMKGEE 79

M.thermo    TGEVLMVAYMNREALRRTLETGTAHYWSTSRGKLWLKGES 72

      ruler .....50.....60.....70.....80

                * :**:* :*: ******::: *** * *** ** ***:.

M.vannielii SKNVQKVLEVFKDCDGDALLFIVEQTGWACHEGYMSCFHN 119

M.thermo    SGHVQRVKDVLVDCDGDAVVLKVEQEGGACHTGYRSCFYR 112

      ruler .....90.....100.....110.....120

                .:* :      ::. : *  :

M.vannielii KVDLN----TGNSTVIGDKLD----- 136

M.thermo    SIDGDELKVREDAVKVFDPEEIYGDG 138

      ruler .....130.....140.....
```

Figure 1.
Highly Conserved Regions of PR-AMP Cyclohydrolase. A.) Alignment highlights twelve of the most highly conserved residues in the cyclohydrolase enzymes. B.) Pairwise alignment of *M. thermoautotrophicum* and *M. vannielii.*

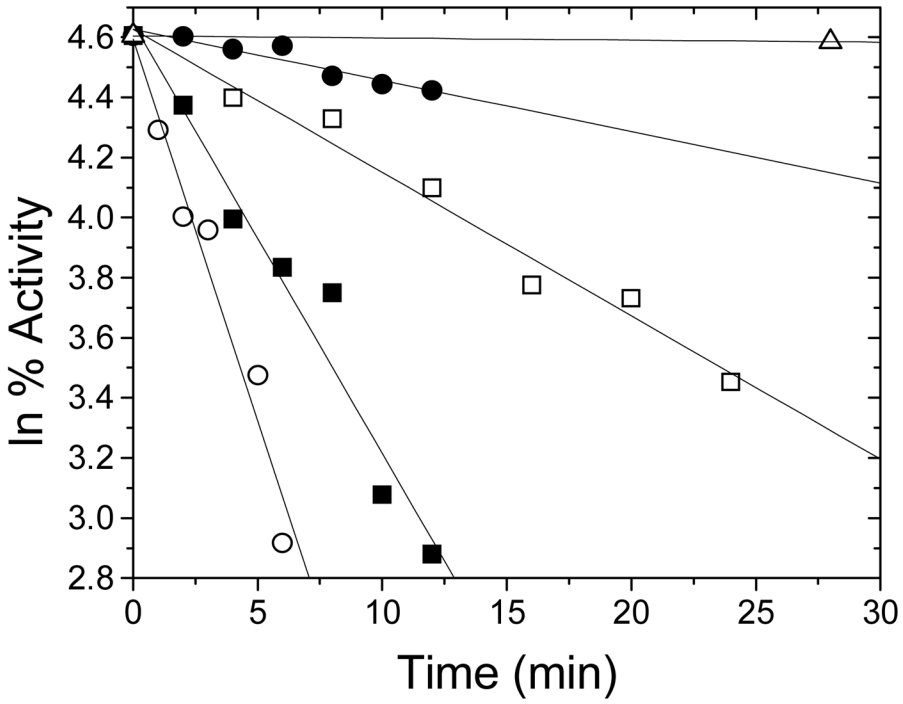

Figure 2.

MMTS Inactivation of PR-AMP Cyclohydrolase and Effect of Substrate on Reactivity of Cysteines. Data are as follows (△) not determined, control no MMTS; (●) 1.7×10^{-2} min^{-1}, 78 μM MMTS, 1.1 mM PR-AMP; (□) 4.8 $x10^{-2}$ min^{-1}, 39 μM MMTS; (■) 1.5 $X10^{-1}$ min^{-1}, 59 μM MMTS; (○) 2.6×10^{-1} min^{-1}, 78 μM MMTS.

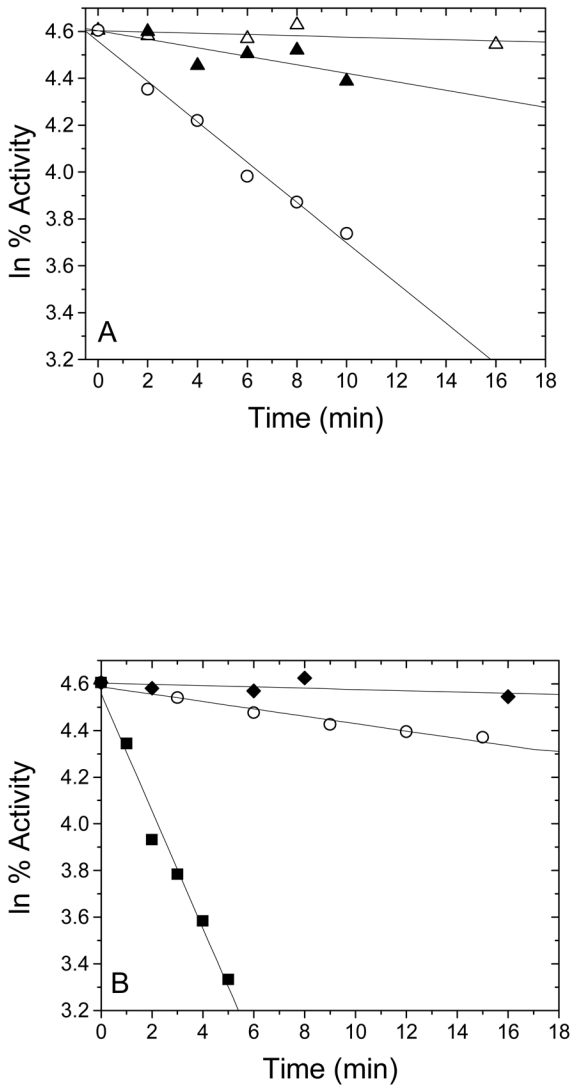

Figure 3.

DTNB Inactivation Rates of PR-AMP Cyclohydrolase and the Effect of PR-AMP and Mg^2. Data are as follows A. (△) 2.7×10^{-3} min^{-1}, control no DTNB, (○) 8.5×10^{-2} $min^{-1,}$ 212 μM DTNB, (▲)1.82 $x10^{-2}$ min^{-1}, 212 μM DTNB with 1.0 mM PR-AMP; B. (◆) 2.7×10^{-3} min^{-1}, control no DTNB, (○) 1.6×10^{-2} min^{-1}, in the absence of Mg^{2+}, 424 μM DTNB, (■) 2.5×10^{-1} min^{-1}, 424 μM DTNB.

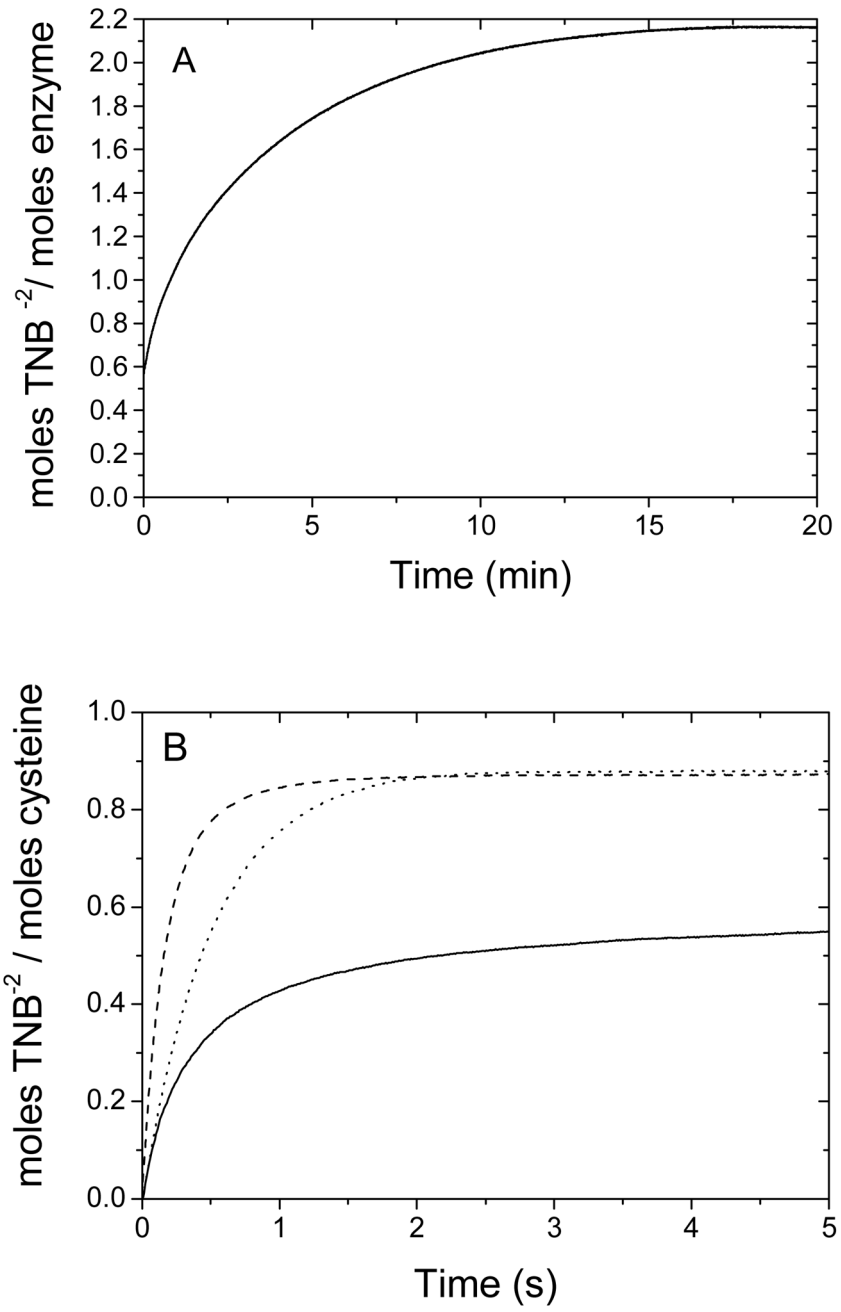

Figure 4.

Stoichiometry and Kinetics of Cyclohydrolase Reaction with DTNB. A.) PR-AMP cyclohydrolase complete reaction with DTNB. Conditions 50 mM Tris-HCl pH 8.5, 1mM EDTA, 5 mM $MgCl_2$ 30°C 625 μM DTNB, and 12.5 μM PR-AMP cyclohydrolase. B.) Stopped-flow results for the reaction of DTNB with native PR-AMP cyclohydrolase (solid line), cysteine (dots), and C109/116A (dashes). Conditions 50 mM KH_2PO_4 pH 7.3, 0.5 mM EDTA 1mM $MgCl_2$ 20ºC 440 μM DTNB 8.7 μM PR-AMP cyclohydrolase.

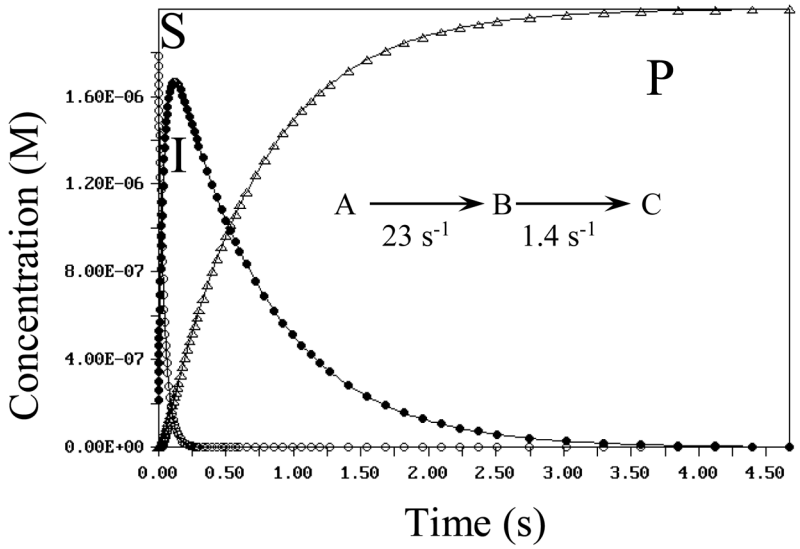

Figure 5.

Stopped flow analysis of the PR-AMP Cyclohydrolase enzymatic conversion: Plots (averages of triplicate runs) of the time vs. concentration for substrate, product and potential intermediate from global fit of the data to a two-step model A>B>C. Open circles (○) are substrate(S), closed circles (●) are intermediate (I), and open triangles (△) are product (P) as labeled.

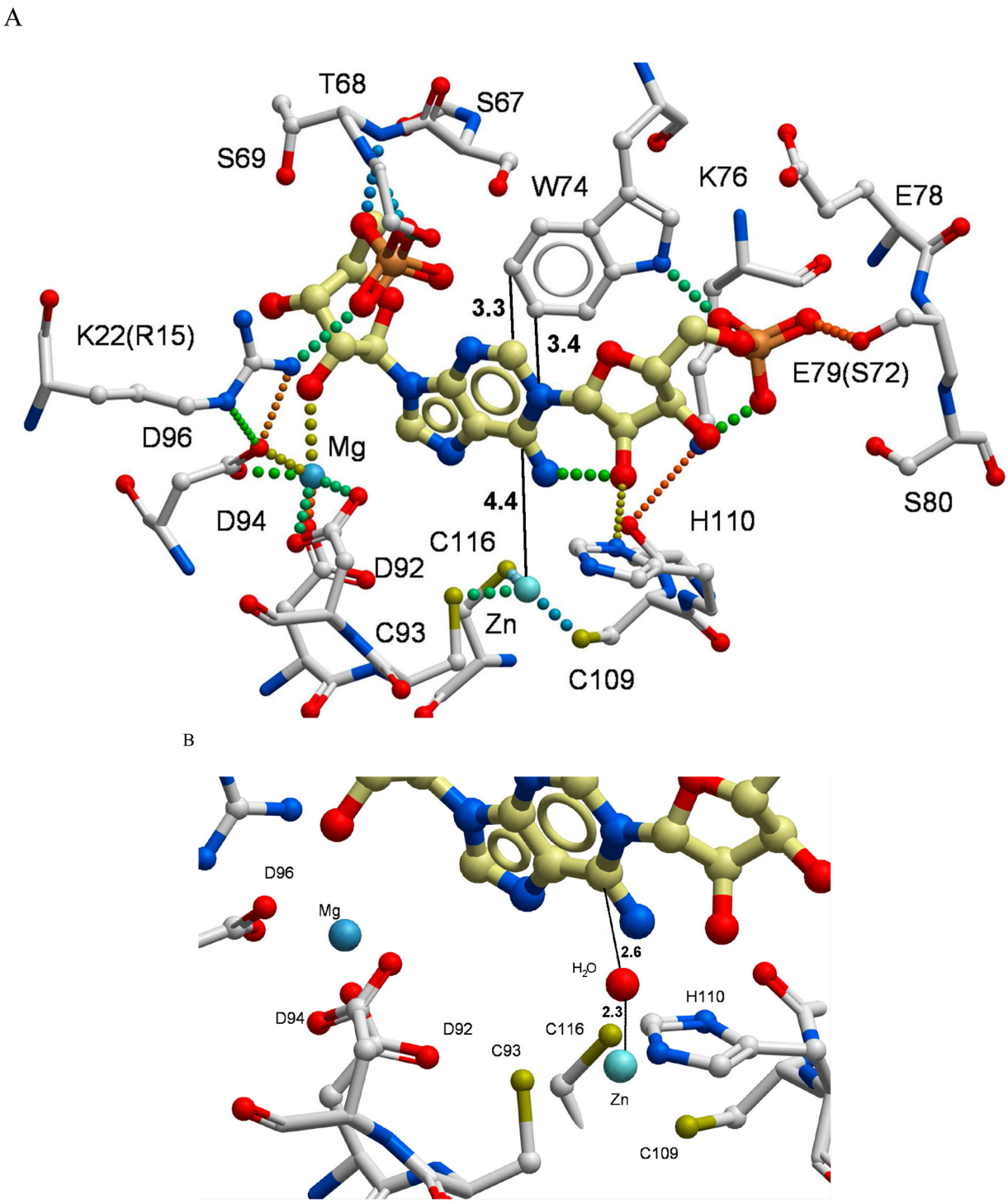

Figure 6.

A structural model of the PR-AMP cyclohydrolase active site with substrate docked. (A) The metal Zn^{2+} and Mg^{2+} binding sites and their relationships to the conserved amino acid residues are indicated to assess the functional roles in substrate binding site. The 16 residues labeled in the figure are among the most highly conserved residues described in Figure 1 and reside within 4 Å of the substrate binding site. (B) To better understand the potential

positioning of the active site for a zinc-activated water attack on the C6 of the purine ring, a molecule of water was manually positioned into the substrate-docked model. Distances (black dotted lines) are shown in angstroms (Å). Hydrogen bonds and coordinative bonds to metals are rendered as colored spheres.

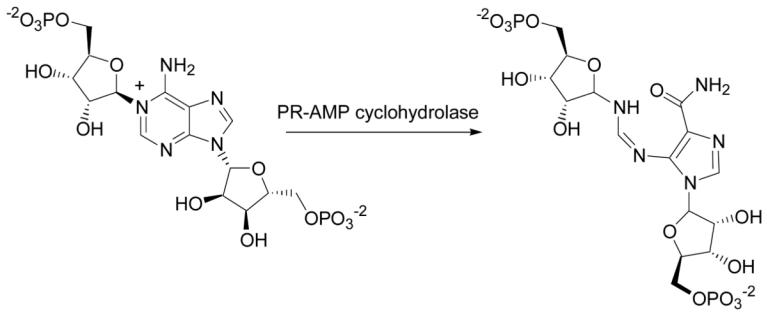

Scheme 1.
Conversion of PR-AMP to 5'-ProFAR by PR-AMP Cyclohydrolase

RSSR is DTNB.

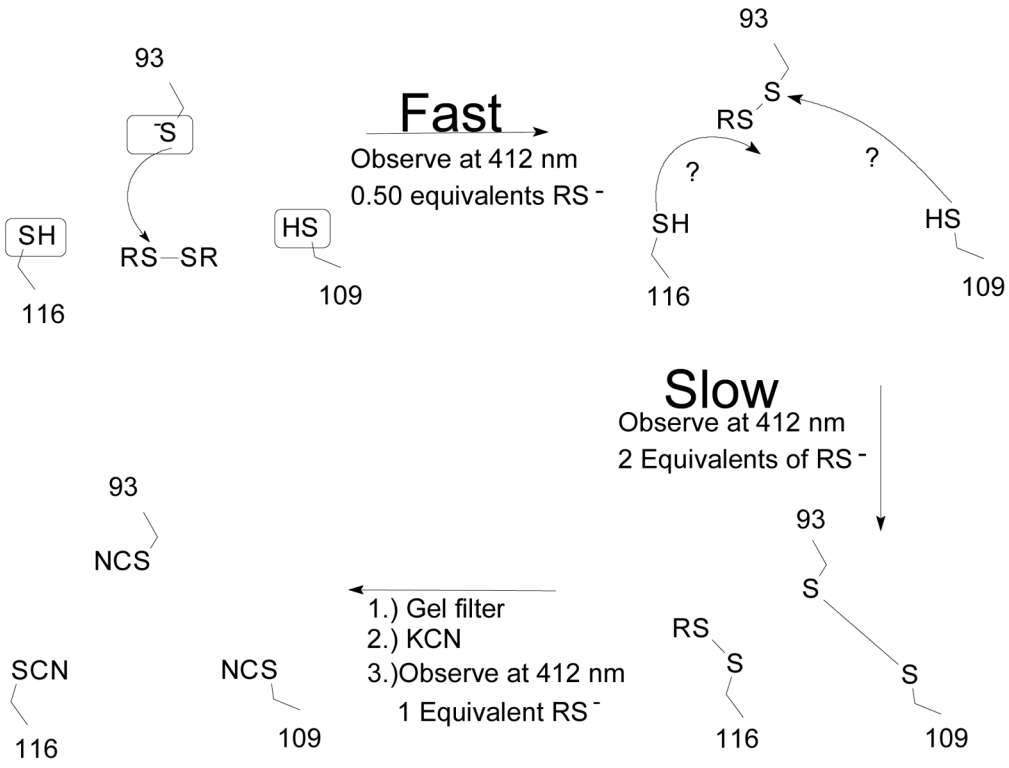

Scheme 2.
Potential Model for Cysteine Reactivity Observed with Native PR-AMP Cyclohydrolase.

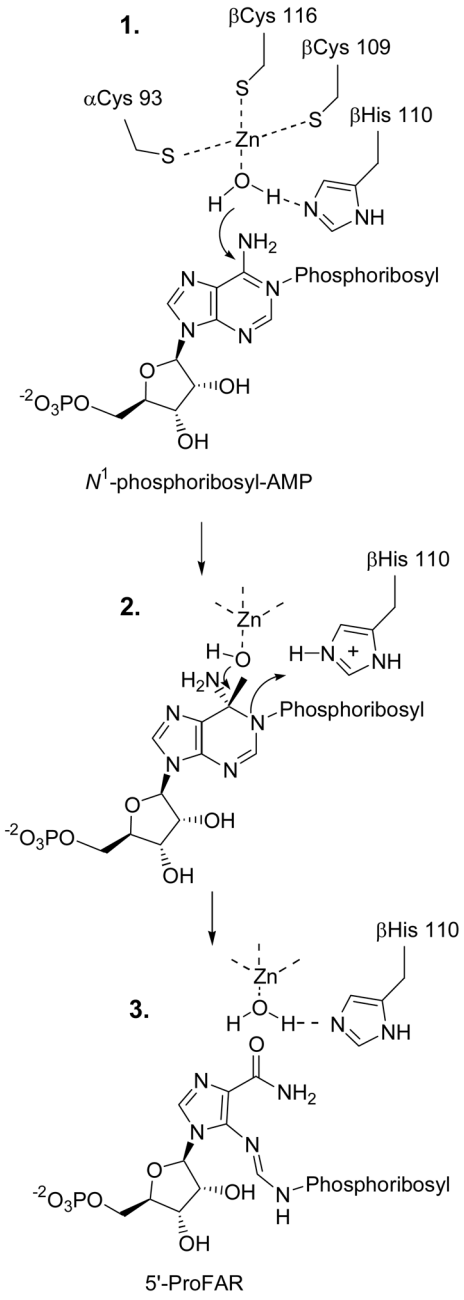

Scheme 3.
Proposed catalytic mechanism for PR-AMP Cyclohydrolase

Table 1

Stoichiometry of Reaction with DTNB.

Native Cyclohydrolase (Specific Activity) U/mg	Stoichiometry (TNB^{2-}/subunit)	Stoichiometry (KCN release/subunit)
10.2	1.12±0.01	0.52±0.01
13.1	1.60±0.10	0.65±0.03
18.1	1.98±0.15	0.72±0.05.

Table 2

Zinc Content and Kinetics of PR-AMP Cyclohydrolase Preparations

Enzyme Species	Zn^{2+} (moles/subunit)	k_{cat}/K_m (M^{-1} s^{-1})
PR-AMP Cyclohydrolase	1.1, 0.88, 1.07	$4.1 \pm 0.8 \times 10^5$
D92E	0.72, 0.51	$2.3 \pm 0.2 \times 10^3$
C93A	0.003, 0.020	Inactive
D94A	0.60, 0.43	Inactive
D94E	0.65, 0.63	$1.8 \pm 0.2 \times 10^2$
C109A	0.37, 0.22	Inactive
H110A	1.16, 1.09	$8.3 \pm 2 \times 10^2$
C116A	0.99, 0.90	Inactive
C109/116A	0.027, 0.007	Inactive
DTNB or MMTS*	0.27, or 0.19*, 0.52*	

The average percent deviation for the independent Zn^{2+} measurements is 10%.

Table 3

Stoichiometry of Reactions with DTNB.

Species	Stoichiometry (TNB^{2-}/subunit)
C93A	0[a]
C109A	0.30±0.03
C116A	0.64±0.02
C109/116A	0.87± 0.08
Wild type[b]	1.98±0.15

[a] No change in absorbance was observed.

[b] Specific activity 18 U mg^{-1}, all other species were catalytically inactive.

Table 4

Stopped-Flow Comparison of DTNB reactions

Source	Rate constant[a] (min^{-1}) pH 7.3	Rate constant[a] (min^{-1}) pH 8.5
Wild type	246	930
Cysteine	120	324
C109/116A	360	3384

[a] Apparent first order rate constants. Conditions as described in experimental except as noted.